Multimodal Imaging of Brain Connectivity Using the MIBCA Toolbox: Preliminary Application to Alzheimer's Disease

Article *in* IEEE Transactions on Nuclear Science · June 2015

DOI: 10.1109/TNS.2015.2417764

CITATION
1

READS
78

4 authors:

Andre Santos Ribeiro
Imperial College London
26 PUBLICATIONS **79** CITATIONS
SEE PROFILE

Luis Miguel Lacerda
University College London
13 PUBLICATIONS **120** CITATIONS
SEE PROFILE

Nuno Andre da Silva
Luz Saúde
17 PUBLICATIONS **20** CITATIONS
SEE PROFILE

Hugo Alexandre Ferreira
University of Lisbon
144 PUBLICATIONS **1,587** CITATIONS
SEE PROFILE

Multimodal Imaging of Brain Connectivity Using the MIBCA Toolbox: Preliminary Application to Alzheimer's Disease

André Santos Ribeiro, Luís Miguel Lacerda, Nuno André da Silva, and Hugo Alexandre Ferreira for the Alzheimer's Disease Neuroimaging Initiative

***Abstract*—The Multimodal Imaging Brain Connectivity Analysis (MIBCA) toolbox is a fully automated all-in-one connectivity analysis toolbox that offers both pre-processing, connectivity, and graph theory analysis of multimodal images such as anatomical, diffusion, and functional MRI, and PET. In this work, the MIBCA functionalities were used to study Alzheimer's Disease (AD) in a multimodal MR/PET approach. Materials and Methods: Data from 12 healthy controls, and 36 patients with EMCI, LMCI and AD (12 patients for each group) were obtained from the Alzheimer's Disease Neuroimaging Initiative (ADNI) database (adni.loni.usc.edu), including T1-weighted (T1-w), Diffusion Tensor Imaging (DTI) data, and 18F-AV-45 (florbetapir) dynamic PET data from 40-60 min post injection (4x5 min). Both MR and PET data were automatically pre-processed for all subjects using MIBCA. T1-w data was parcellated into cortical and subcortical regions-of-interest (ROIs), and the corresponding thicknesses and volumes were calculated. DTI data was used to compute structural connectivity matrices based on fibers connecting pairs of ROIs. Lastly, dynamic PET images were summed, and the relative Standard Uptake Values calculated for each ROI. Results: An overall higher uptake of 18F-AV-45, consistent with an increased deposition of beta-amyloid, was observed for the AD group. Additionally, patients showed significant cortical atrophy (thickness and volume) especially in the entorhinal cortex and temporal areas, and a significant increase in Mean Diffusivity (MD) in the hippocampus, amygdala and temporal areas. Furthermore, patients showed a reduction of fiber connectivity with the progression of the disease, especially for intra-hemispherical connections. Conclusion: This work shows the potential of the MIBCA toolbox for the study of AD, as findings were shown to be in agreement with the literature. Here, only structural changes and beta-amyloid accumulation were considered. Yet, MIBCA is further able to process fMRI and different radiotracers, thus leading to integration of functional information, and supporting the research for new multimodal biomarkers for AD and other neurodegenerative diseases.**

***Index Terms*—Alzheimer's Disease, brain connectivity, graph theory, image processing, magnetic resonance imaging, molecular imaging, multimodal imaging, network theory, positron emission tomography, toolbox.**

Manuscript received September 30, 2014; revised January 25, 2015; accepted March 12, 2015. Date of publication May 08, 2015; date of current version June 12, 2015. This work was supported in part by Fundação para a Ciência e Tecnologia (FCT) and Ministério daCiência e Educação (MCE) of Portugal (PIDDAC) under Grant PTDC/SAUENB/120718/2010 and Grant PEst-OE-/SAU/UI0645/2014. Data used in preparation of this paper were obtained from the Alzheimer's Disease Neuroimaging Initiative (ADNI) database (adni.loni.usc.edu). As such, the investigators within the ADNI contributed to the design and implementation of ADNI and/or provided data but did not participate in analysis or writing of this paper. A complete listing of ADNI investigators can be found at: http://adni.loni.usc.edu/wp-content/uploads/how_to_apply/ADNI_Acknowledgement_List.pdf.

A. Santos Ribeiro is with the Centre for Neuropsychopharmacology, Division of Brain Sciences, Department of Medicine, Imperial College London, London W12 0NN, U.K., and also with the Institute of Biophysics and Biomedical Engineering of the Faculty of Sciences of the University of Lisbon, Lisboa 1749-016, Portugal (e-mail: a.santos-ribeiro13@imperial.ac.uk).

L. M. Lacerda is with the Centre for Neuroimaging Sciences, Institute of Psychiatry, Psychology, and Neuroscience, King's College London, London SE5 8AF, U.K., and also with the Institute of Biophysics and Biomedical Engineering, Faculty of Sciences, University of Lisbon, Lisboa 1749-016, Portugal (e-mail: luis.lacerda@kcl.ac.uk).

N. A. da Silva is with the Institute of Neuroscience and Medicine-4, Forschungszentrum Juelich GmbH, Juelich 52425, Germany, and also with the Institute of Biophysics and Biomedical Engineering, Faculty of Sciences, University of Lisbon, Lisboa 1749-016, Portugal (e-mail: n.da.silva@fz-juelich.de).

H. A. Ferreira is with the Institute of Biophysics and Biomedical Engineering, Faculty of Sciences, University of Lisbon, Lisboa 1749-016, Portugal (e-mail: hhferreira@fc.ul.pt).

This paper has supplementary downloadable material available at http://ieeexplore.ieee.org.

Color versions of one or more of the figures in this paper are available online at http://ieeexplore.ieee.org.

Digital Object Identifier 10.1109/TNS.2015.2417764

I. Introduction

NEUROIMAGING techniques have long been used to unfold the complexity of human brain anatomy and function. The neuroimaging technique of election to study brain connectivity is Magnetic Resonance Imaging (MRI). MRI allows measuring *in vivo* and non-invasively the human morphology, structure and dynamics with high resolution and soft tissue contrast. Further, MRI has been extensively used in the context of structural connectivity, where the measurement of the random displacement of water molecules using diffusion MRI (dMRI) allows the tracing of three-dimensional paths between different brain regions via tractography [1], [2]. Functional connectivity, on the other hand, typically uses functional MRI (fMRI), which has helped undercover concepts about the basal level of activations in the brain (resting state networks) [3], [4].

However, MRI lacks molecular sensitivity and specificity, when compared with Nuclear Medicine methods such as Positron Emission Tomography (PET), which allows acquiring quantitative molecular data. Furthermore, the broad spectrum of radiotracers allows understanding diseases states of different molecular pathways. On the other hand, PET presents low spatial resolution and reduced anatomical information. The combination of complementary information from multimodal data is therefore highly desired. In fact, it has already been

shown that multimodal data brings new perspectives to the knowledge of the brain and in particular it has been used to find biomarkers for neurological diseases, such as Alzheimer's Disease (AD) [5], [6].

Nonetheless, managing and processing such multimodal data is not straightforward and it is time consuming. Moreover, processing is often performed in a non-automatic manner that is prone to human error. Current automatic multimodal methods are still fairly limited, being majorly focused on one technique [7]–[9].

In this paper we exploit the multimodal capability of the fully automated all-in-one connectivity analysis toolbox - Multimodal Imaging Brain Connectivity Analysis toolbox (MIBCA). MIBCA offers pre-processing, connectivity and graph theory analyses, and visualization of multimodal data such as anatomical MRI (aMRI), dMRI, fMRI and PET. Here, MIBCA was applied to AD as a preliminary proof-of-concept study.

II. Materials and Methods

In this section the ADNI database will be firstly described, followed by the description of the subject groups, the neuroimaging sequences and the protocols used. Further, the neuroimaging data processing and analysis performed by the MIBCA toolbox will be introduced.

A. ADNI database

Data used in the preparation of this article were obtained from the ADNI database (adni.loni.usc.edu). To date, over 1500 adults, aged 55 to 90, were recruited to participate in the research, consisting of cognitively normal older individuals, patients with early or late Mild Cognitive Impairment (MCI), and patients with AD. For up-to-date information, see www.adni-info.org.

In this study, a total of 48 subjects of the ADNI-2 database presenting concurrently volumetric T1-weighted (T1-w), Diffusion Tensor Imaging (DTI) and PET data were studied. Subjects belonged to 4 groups according to ADNI baseline diagnosis: healthy controls (CTRL); and early MCI (EMCI), late MCI (LMCI) and AD patients. Demographic data (age and gender), Apolipoprotein E (ApoE) genotyping - absolute frequency (2/3, 3/3, 3/4 and 4/4) - and Mini-Mental State Examination (MMSE) are shown in Table I.

TABLE I
Demographic, Genetic and Neuropsychological Characterization of Subject Groups

	CTRL	EMCI	LMCI	AD
N	12	12	12	12
Gender	5F/7M	4F/8M	6F/6M	3F/9M
Age[a] (y.o.)	74.5±8.8 [64-90]	71.8±7.3 [55-82]	70.9±7.0 [57-83]	75.3±7.8 [60-89]
ApoE	2/3: 1 3/3: 6 3/4: 4 4/4: 1	2/3: 2 3/3: 3 3/4: 5 4/4: 2	2/3: 0 3/3: 2 3/4: 8 4/4: 2	2/3: 1 3/3: 6 3/4: 5 4/4: 0
MMSE	29.2±1.2 [26-30][b]	28.7±1.2 [26-30][c]	26.5±2.0 [24-30][b,c,d]	23.6±1.8 [21-26][b,c,d]

F = Female; M = Male

[a]Age at the time of diagnostic screening and imaging: mean ± standard deviation and age range (y.o. = years old). ApoE genotyping; MMSE = Mini-Mental State Examination: mean ± standard deviation scores and scores ranges; Kruskal-Wallis test: significant difference in MMSE (p=0.000); individual Mann-Whitney tests: [b]significant difference between CTRL group and LMCI (p=0.001) and AD (p=0.000) patient groups; [c]significant differences between EMCI and LMCI (p=0.007), and AD (p=0.000) patient groups; [d]significant difference between LMCI and and AD (p=0.003) patient groups; No additional significant differences were observed between subject groups.

F = Female; M = Male
[a] Age at the time of diagnostic screening and imaging: mean ± standard deviation and age range (y.o. = years old). ApoE genotyping; MMSE = Mini − Mental State Examination: mean ± standard deviation scores and scores ranges; Kruskal-Wallis test: significant difference in MMSE (p = 0.000); individual Mann-Whitney tests:
[b] significant difference between CTRL group and LMCI (p = 0.001) and AD (p = 0.000) patient groups;
[c] significant differences between EMCI and LMCI (p = 0.007), and AD (p = 0.000) patient groups;
[d] significant difference between LMCI and and AD (p = 0.003) patient groups; No additional significant differences were observed between subject groups.

B. Neuroimaging data

MRI data including high-resolution T1-w and DTI data were acquired using a 3T MRI scanner (Discovery MR750, General Electric, Milwaukee, U.S.A.) and an 8-channel receive-only head coil. T1-w sequence (IR-SPGR) parameters include: sagittal plane; Slices = 196; TR/TE/TI = 7.3/3.1/16 ms; FA = 11°; Matrix = 256 × 256; Voxel size = 1.0 × 1.0 × 1.2 mm^3. DTI sequence (spin echo with echo planar readout): axial plane; Slices = 60; 41 non-colinear diffusion-sensitizing gradient directions; b = 0, 1000 s/mm^2 with 5 b0 acquisitions; TR/TE = 190/62 ms; FA = 90°; Reconstruction matrix = 256 × 256; Voxel size = 1.4 × 1.4 × 2.7 mm^3.

In addition, a hybrid PET/Computed Tomography scanner (Siemens, Erlangen, Germany) was used to acquire 18F-AV-45 (florbetapir) dynamic PET data from 40-60 min post injection (4 × 5 min frames). PET data were acquired with the following parameters: Slices = 109; Matrix = 336 × 336; Voxel size = 1.0 × 1.0 × 2.7 mm^3; frames = 4. Data were attenuation, decay, random, and scatter corrected and reconstructed using OSEM2D with 4 iterations and 16 subsets.

C. MIBCA Toolbox

The MIBCA toolbox is an application developed in MATLAB. The toolbox combines and integrates multiple freely available and referenced neuroimaging software packages and applications in order to optimize and automate data processing within a multimodal imaging framework for brain connectivity analysis [10], [11]. Combined neuroimaging tools include Freesurfer [12], FSL [13], SPM [14], Diffusion Toolkit [15] and the Brain Connectivity Toolbox [16]. Currently, the MIBCA toolbox is able to process aMRI from high-resolution T1-w images, dMRI from DTI, fMRI from blood oxygen level dependent (BOLD) resting-state or task-related data (not used in this study) and also PET data of distinct radiotracers [17]. The data processing (C.1) and analysis (C.2) performed on this study is explained below and summarized in Table II.

1) Data Processing: Following a data folder hierarchy "Study-Subject-Acquisition-Images" the toolbox automatically

TABLE II
ANALYSED MODALITIES AND ASSOCIATED PRE-PROCESSING AND EXTRACTED METRICS

Modality	Pre-processing	Metrics
aMRI	Intensity normalization; skull stripping; affine and non-linear registration to the MNI305 atlas; segmentation into gray and white-matter and cerebro-spinal fluid; cortical and subcortical parcellation.	Cortical thickness, gray-matter volume
DTI	Eddy current correction; diffusion tensor reconstruction; FACT fiber tracking estimation; registration to aMRI	Mean Diffusivity, Fractional Anisotropy, fiber count, node degree, clustering coefficient
PET	Motion correction; 8 mm Gaussian smoothing; relative Standard Uptake Values estimation; registration to aMRI	Relative Standard Uptake Values

identifies and processes the different subjects in batch and specifically for each modality. Due to the specificities of each imaging modality, these will be discussed next.

aMRI is the first modality to be processed by the toolbox. This is the only modality that is required to be processed first as it defines the non-linear transform (subject-template) that is further applied in all other modalities. Using pipelined Freesurfer, the following pre-processing steps were applied: non-parametric non-uniform intensity normalization; skull stripping; affine and non-linear registration to the MNI305 atlas; segmentation into gray and white-matter and cerebro-spinal fluid; and parcellation into cortical and subcortical regions-of-interest (ROIs) according to the Desikan-Killiany-Tourville atlas. The imaging metrics used in this study, including cortical thickness (CThk), and gray matter volume (GMV) for cortical ROIs and GMV for subcortical ROIs, are then collected and organized from Freesurfer output using a specific toolbox script.

Diffusion images were first corrected for eddy currents using eddy_correct function (corrects for eddy current-induced distortions and subject movements; available through FSL), and the diffusion tensor was reconstructed from the raw images using dti_recon function (available through Diffusion Toolkit). From the reconstructed images, the Mean Diffusivity (MD) and Fractional anisotropy (FA) maps were produced. Deterministic fiber tracking was also performed with the diffusion toolkit using the Fiber Assignment by Continuous Tracking (FACT) algorithm to generate the streamlines from diffusion data. The T1-w image was then affine registered to the b0 diffusion image, and the transformation applied to the atlas image registered to the T1-w (obtained through the aMRI pipeline). The registered atlas image is then used to extract the mean MD, FA and fiber count for each ROI.

PET images were first corrected for motion using SPM and smoothed with an 8 mm Gaussian filter. The summed activity was obtained from the dynamic PET data and affine registered to the T1-w image. The aligned ROIs were then mapped back to the PET space. The summed image was then transformed to relative Standard Uptake Values (rSUV) with the cerebellum as the reference ROI. The registered atlas image was once more used to extract the mean rSUV for each ROI.

2) Data Analysis: For each extracted metric the average and standard deviation value for each of the studied groups (CTRL, EMCI, LMCI, and AD) was automatically obtained.

Additionally, from fiber tracking data, structural connectivity matrices were automatically computed by determining the number of fibers connecting each ROI pair (FiberConn).

Then, using Graph theory analysis, the node degree (Deg) and clustering coefficient (ClusC) metrics were calculated from the matrices. Deg represents the number of regions to which a particular region is connected to, and thus translates how much that region is integrated or communicates with different networks. ClusC of a region represents the fraction of that region's neighbours (i.e. to which the region is connected to) that are neighbours of each other, and therefore translates how segregated is a particular region and associated network regarding others. This segregated network may correspond, for instance, to a particular brain function.

D. Statistical Analysis

Subject group demographic data (age and gender), ApoE genotype and MMSE scores were analysed regarding mean, standard deviation, and range values, and regarding absolute frequencies when appropriate. Subject groups (controls and patients) where compared regarding age and MMSE using Kruskal-Wallis and Mann-Whitney U tests, and Gender and ApoE genotype using the Chi-square test. Non-parametric tests were used due to the low number of subjects per group. The statistical analysis was done using PASW Statistics 21 software and a significance of $p < 0.05$ was used.

Statistical differences between each 2 groups were computed directly by the toolbox for each imaging and connectivity metric and also for FiberConn. Here, the Mann-Whitney U test with $p < 0.05$ was also used whilst controlling for age and gender.

Summarizing, the analysed metrics for this study were: CThk and GMV from aMRI; MD, FA, Deg, ClusC and FiberConn from dMRI and rSUV from 18F-AV-45 data.

III. RESULTS AND DISCUSSION

In this section group characterization will be firstly discussed regarding values and statistical tests performed. Then connectivity results and imaging metrics will be presented and discussed for each group comparison (e.g. CTRL vs EMCI). Finally, an overall discussion will be done regarding findings for all groups studied.

A. Group characterization

It can be seen from Table I that MMSE scores decrease monotonically from the CTRL to the EMCI, LMCI and AD patient groups, as expected. In fact a highly significant overall difference in MMSE was found using Kruskal-Wallis test ($p = 0.000$). Individual comparisons between group pairs using the Mann-Whitney test hold also significant differences ($p < 0.010$) with the exception of CTRL vs EMCI with no observable significant difference.

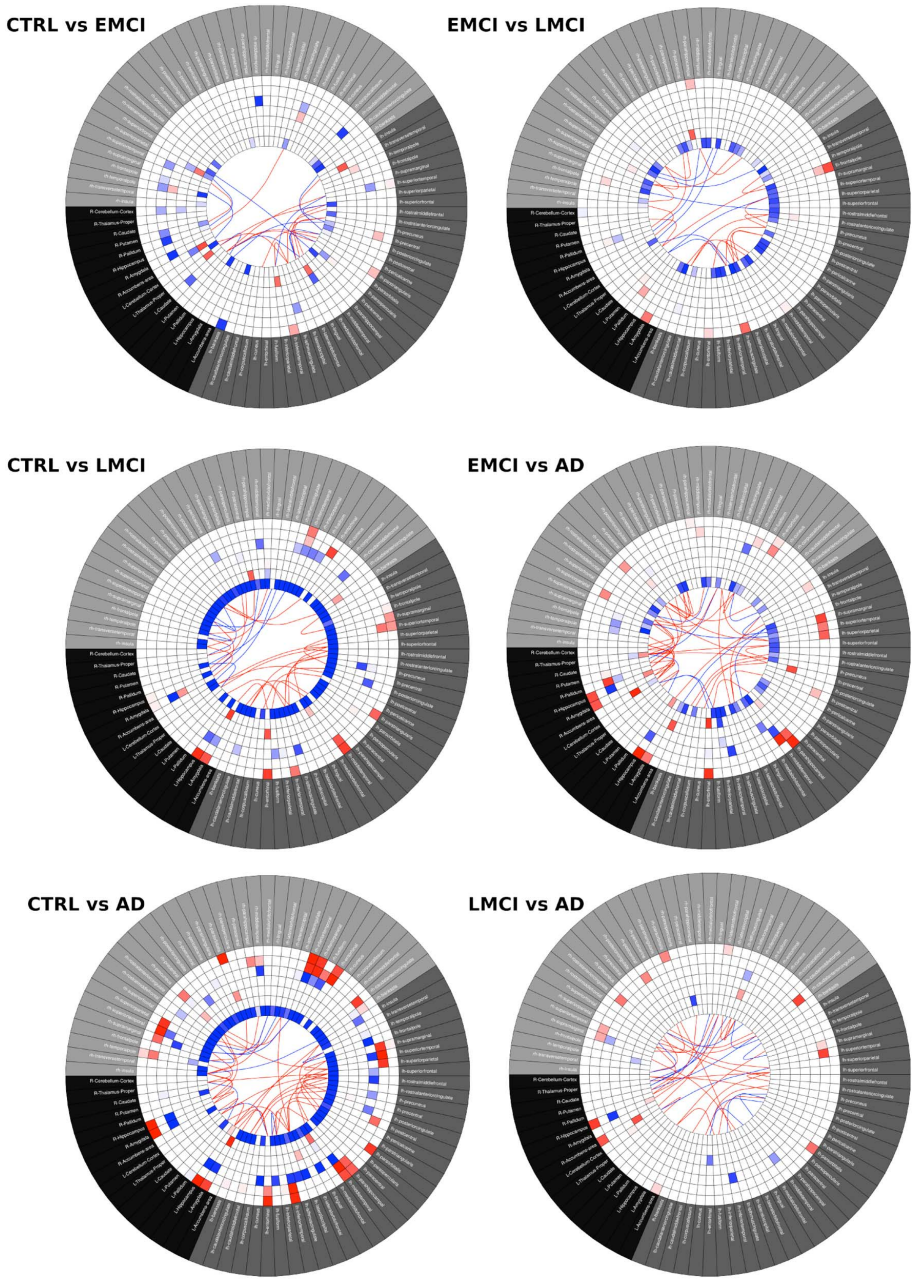

Fig. 1. Connectograms for CTRL vs (EMCI, LMCI and AD), for EMCI vs (LMCI, and AD), and for LMCI vs AD. The outermost rings represent Freesurfer T1-weighted segmented cortical (right hemisphere–light gray; left hemisphere–darker gray) and subcortical (black) brain regions. The inner rings from the outermost to the innermost respectively represent gray matter volume, cortical thickness, mean diffusivity, fractional anisotropy, node degree and clustering coefficient of the structural DTI matrix, and PET relative standard uptake value. Red and blue squares respectively represent significant lower or higher values of the corresponding ring metric for the second group in comparison to the first. In the center is a representation of structural DTI connectivity (fibers connecting different brain regions). Red and blue lines respectively represent significantly decreasing or increasing number of fibers between groups. Here more intense colors represent higher significances and therefore larger group differences. The Mann-Whitney U test was applied with significance $p < 0.05$. (see supplementary material for a higher magnification of this image).

This exception is to be expected if one considers that often small differences in the clinical assessment and the limitations of neuropsychological testing can result in one subject being classified in one or another group, especially when clinical findings are subtle and diagnosis is unsure as is the case of patients with EMCI [12]. Additionally, statistical tests showed that the 4 groups are age- (Kruskall-Wallis and Mann-Whitney tests), gender and ApoE genotype matched (Chi-square tests), meaning that differences between groups found in the following analysis should arise from pathology only and/or other co-variables herein not considered. This is crucial since age, for example, has been proven to confound the effect of AD in specific regions along the cortical surface [18], [19].The multimodal imaging connectivity group comparison analysis is presented in Fig. 1 and Table III, and will be discussed further below.

B. Connectivity Analysis CTRL vs EMCI

Even though, no significant differences were observed between groups regarding demographics, ApoE genotyping and MMSE scores, differences in several temporal lobe regions were observed regarding different imaging and connectivity metrics. Particularly, the left hemispherical (Lh) inferior temporal gyrus (ITG) showed a decrease in GMV and the superior temporal gyrus (STG) showed a decrease in GMV and also an increase in MD. The right hemispherical (Rh) ITG and the temporal pole (TP) both showed an increase in MD and a decrease in FA, and the Rh STG showed only an increase in MD. All the identified temporal regions are known to be affected in AD, namely regarding the loss of gray-matter and tissue architecture resulting in a decrease in GMV and an increase in MD [20]. A decreasing structural connectivity was also observed for the Rh-STG and the Hippocampus (Hip). In fact, for the Hip, changes were observed in white-matter (decrease in the number of tracts) whilst no GMV changes were observed which agrees with a recent work, where it was observed that white-matter changes precede hippocampal atrophy in EMCI patients [21].

Additionally, an increase in Deg and a decrease in ClusC were observed for the Lh medial orbito-frontal cortex (MeOFC) and Rh superior parietal lobule (SPL) and Nucleus Accumbens (Acc). The Rh-SPL also showed an increased rSUV, consistent with the uptake of the beta-amyloid specific 18F-AV-45 tracer. These regions are also known to be affected in AD [20], [22], [23]. In particular, structural changes in the orbitofrontal cortex have been observed in patients with MCI and AD 4 years before any cognitive symptoms [24]. Interestingly, in this work changes were identified using the connectivity metrics but not the imaging metrics, suggesting that the former may be more sensitive to particular tissue structural changes than imaging metrics. More recent studies have validated this finding and further evaluated the use of different features in the differentiation between MCI and AD groups, and controls, suggesting improvements in the accuracy of the classification when using network measures [25], [26]. The fact that Deg increases and ClusC decreases may suggest that these regions establish additional connections with regions other than the ones from the traditional network as a means to compensate other brain regions losses. Given the small studied groups further studies would be necessary to confirm this hypothesis.

C. Connectivity Analysis CTRL vs LMCI

It can be observed from the connectograms in Fig. 1 that differences between groups were more extensive. In particular, changes in additional temporal lobe regions associated with AD were observed, including the: ITG, STG and middle temporal gyrus (MTG), Hip, Amygdala (Amg), and entorhinal cortex (ERC). Also, other regions known also to be changed in AD were observed, including: the fusiform gyrus (FG) bilaterally, the supramarginal gyrus (SMG), the inferior parietal lobule (IPL), the precuneus (PCn) and the frontal pole (FP) [27].

Again, the connectivity metrics identified changes regarding the Deg and ClusC of the MeOFC. Intriguingly, the Rh-MeOFC showed an opposite behaviour to what was described before for the Lh-MeOFC: a decrease in Deg and an increase in ClusC. This fact could be interpreted as a region losing some of the connections to the outside of its nearest- neighbour network, resulting in an increased segregation. Nonetheless, an overall decrease/increase in structural connectivity was observed in the Lh/Rh, respectively. It is also worth considering that although AD causes cell atrophy locally and it might have a specific pattern of progression which affects the white matter tracts in different ways [28], some studies, have actually reported different results in connectivity for the same regions [29].

Additionally, an overall rSUV increase was observed in the patient group, with the exemption of most basal ganglia structures. Interestingly, the putamen showed also a higher 18-AV-45 uptake which is consistent among patient groups EMCI, LMCI and AD. Uptake changes in the putamen have also been observed in other studies [30], [31].

D. Connectivity Analysis CTRL vs AD

In this comparison, even more pronounced changes comparatively to both CRTL-EMCI and CRTL-LMCI were observed. In fact, several of the regions identified as different between CTRL vs LMCI, were here different as well, and also different in additional metrics. Such are the cases of the Lh-ITG, MTG, SMG, and of the Rh-TP, Hip, ERC, IPL, parahippocampalgyrus (PHG), and several parcels of the middle frontal gyrus (MFG) and the insula (Ins). Most of the changes were observed as GMV and CThk decreases and MD increases [20]. In fact, MD has been identified as a more sensitive measure than FA to identify differences between controls and different groups, such as MCI and AD [32], which might explain why there were changes in MD in more regions than when compared to FA.

As before, the Lh-MeOFC showed an increase in Deg and a decrease in ClusC. Also, a decrease in ClusC was observed for Lh-Hip and Amg, and an increase in ClusC was observed for Rh-TP. Interestingly, the Lh-Hip also showed a decrease in rSUV which suggests an extensive tissue change. Otherwise, the overall increase in rSUV translates the extensive dissemination of beta-amyloid deposition [30].

Lastly, a bilateral decrease in connections with the Hip and with other temporal structures such as the Amg, PHG, STG, MTG, ITG, and TP and also with FP were observed suggesting an extensive compromise of the brain's structural connectivity. This finding is corroborated by previous studies that have implicated changes in cortical regions such as the PHG regarding white matter, which helps explaining and predicting the progression of the disease [33].

E. Connectivity Analysis EMCI vs LMCI

Differences between the EMCI and LMCI groups were observed mainly in the Lh-FP, which could translate the deterioration of cognitive functions as assessed by the MMSE. Additional changes were observed in the MTG, ERC, PHG, Amg and also in the cingulate gyrus and in the basal ganglia: palidum (Pd), putamen (Pt) and thalamus (Tha). These latter changes could also be associated with cognitive decline [34].

Further, the Rh-Tha showed a decrease in ClusC and in rSUV and the Lh-Tha showed a decrease in the number of fibers connecting to the TP. Additional decreases in the number of fiber connections included: Lh-FP and Lh-Ins; Lh-STG and Lh-ITG;

TABLE III
REGIONAL SIGNIFICANT CHANGES IN MULTIMODAL IMAGING METRICS AND CONNECTIVITY PARAMETERS IN SUBJECT GROUPS COMPARISONS

	CTRL vs EMCI	CTRL vs LMCI	CTRL vs AD	EMCI vs LMCI	EMCI vs AD	LMCI vs AD
GMV increases	Lh-Bankstss			Rh-CerebC		
GMV decreases	Lh-**STG**, ITG, parsT	Lh-**Hip**, Amg, **ERC**, ITG, **MTG**, parsT, **STG**, SMG, FP; Rh-ITG, Hip; Amg	Lh-**Hip**, Amg, **ERC**, MTG, **PHG**, parsO, **SMG**; Rh-**ERC**, IPL, ITG, **parsO**, TP, **Hip**, **Amg**	Lh-**FP**,iCG, MTG, ERC, Amg; rh-PHG	Lh-**Hip**, Amg, ERC, PHG; Rh-**ERC**, PHG, **Hip**, Amg	Lh-Acc, parsO; Rh-LOFC, parsO, **Hip**, **Acc**
CThk decreases	Lh-PCG	Lh-**MTG**, **STG**; Rh-ERC, ITG	Lh-Bankstss, caMFG, **ERC**, IPL, ITG, MTG, **PHG**, PoCG, SPL, **STG**, **SMG**; Rh-**Bankstss**, caCG, **ERC**, **FG**, IPL, **MTG**, PHG, PCn, SPL, **STG**, **SMG**, TP,	Lh-**FP**	Lh-**MTG**, PHG, PoCG, SPL, STG, SMG, Ins; Rh-**ERC**,IPL, MTG, PCn, SPL	Lh-STG, SMG; Rh-CaCG, PoCG, raCG, STG, **SMG**
MD increases	Lh-**STG**, Cd, iCG; Rh-**CerebC, TP, ITG**, caMFG, MTG, STG, FP, CerebC, Pt, Pd, Amg	Lh-**Hip**, Amg, caCG, FG, IPL, iCG, pCG; **PCn**; Rh-caMFG, FG, IPL, ITG, iCG, MTG, PCal, Amg	Lh-**Hip**, Amg, FG, iCG, MTG, pCG, PCn, rMFG, SFG, **STG**, TP, Ins; Rh-**Bankstss**, **FG**, IPL, iCG, **MTG**, Pcal, PCn, rMFG, **STG**, Cd, **Hip**, **Amg**	Lh-caCG	Lh-**Hip**, ERC, ITG, **MTG**; Rh-ITG, **Hip**	Lh-ITG, MTG; Rh-**ITG**, **SMG**, **Hip**
MD decreases		Lh-parsO		Lh-Pd; Rh-**Pd,** FP	Rh-Pt, **Pd**	
FA increases		Lh-**PCn**; Rh-parsO	Rh-pCG, **SMG**	Lh-Pt; Rh-**Pd**, raCG,	Lh-**IPL**,MeOFC; Rh-pCG, SMG, FP, TP, **Pd**	
FA decreases	Lh-TP; Rh-**ITG, TP**	Rh-Amg				Lh-CerebC
Deg increases	Lh-**MeOFC**; Rh-**SPL, CerebC, Acc**		Lh-**MeOFC**,			Lh-ERC
Deg decreases	Lh-**parsO**	Lh-**ERC**; Rh-Bankstss, MeOFG	Lh-LOC, PCG, Rh-**parsO**, PCn	Lh-raCG; Rh-SPL	Lh-PCG; Acc Rh-PCG, Acc	Rh-**ITG**, **Acc**
ClusC increases	Lh-**parsO**	Rh-MeOFC	Rh-TP	Rh-Tha	Lh-**IPL**	Rh-PaCG, TP
ClusC decreases	Lh-**MeOFC**; Tha, IPL, Rh-**SPL, Acc**	Lh-Amg, MeOFC; Rh-PaCG	Lh-**Hip**, Amg, **MeOFC**	Rh-parsO	Lh- ERC, PHG,	
rSUV increases	Lh-PCG; Rh-**SPL**, caMFG, Pt, Pd	Overall except most basal ganglia	Overall except most basal ganglia	Lh-MTG, **FP**	Lh-Acc; Rh-Acc	
rSUV decreases			Lh-**Hip**	Rh-Tha,	Lh-**Hip**; Rh-**Hip**, Tha	Rh-**Hip**
FiberConn	Decrease highlight: Rh-STG and Rh-Pt; Rh-Hip and Rh-iCG	Decrease especially within the Lh; increase in the Rh	Bilateral decrease in connections with the Hip and with other temporal structures: Amg, PHG, STG, MTG, ITG, TP and also with the FP	Decrease highlight: Lh-Tha and Lh-TP; Lh-FP and Lh-Ins; Lh-STG and Lh-ITG; Rh-STG and Rh-PCn	Decrease highlight: Rh-Tha; Rh-Acc and Rh-Pt; Increase highlight: Lh-STG and Rh-STG; several interhemispherical connections decreased	Bilateral decreasing and increasing connections; Bilateral decreasing connections with the Hip

The table shows main significant regional increases and decreases in imaging metrics and connectivity parameters for the second group in comparison to the first. Regions with 2 or 3 changes (except rSUV) are displayed in bold, and underlined, respectively. In the rSUV rows are described specific regions or an overall appreciation. SC = structural connectivity; GMV = gray matter volume; CThk = cortical thickness; MD = mean diffusivity; FA = fractional anisotropy; Deg = SC node degree; ClusC = SC clustering coefficient; rSUV = relative standard uptake value; FiberConn = number of fibers connecting pairs of regions (SC); Rh – right hemispherical; Lh – left hemispherical; acronym suffixes G = gyrus, L = lobule, C = cortex, and P = pole; ITG = inferiortemporal; MTG middletemporal; STG = superiortemporal; TTG = transverse temporal; SMG = supramarginal; SPL = superior parietal; IPL = inferiorparietal; LG = lingual; FG = fusiform; TP = temporal; FP = frontal; MeOFC = medial orbito-frontal; LOFC = lateral orbito-frontal; rMFG = rostral middle frontal; SFG = superior frontal; LOFG = lateral orbitofrontal; LOG = lateral occipital; iCG = isthmus of the cingulate; caCG = caudal-anterior cingulate; raCG = rostral-anterior cingulate; pCG = posterior cingulate caMFG = caudal middle frontal; PHG = parahippocampal; parsO = pars orbitalis; parsT = pars triangularis; parsOp = pars opercularis; PCal = pericalcarine; ERC = entorhinal; Amg = amygdala; Hip = hippocampus; Acc = accumbens; Cd = caudate; Pd = pallidum; Pt = putamen; Tha = thalamus; Ins = Insula; Cn = cuneus; PCn = precuneus; PCG = precentral; PaCG = paracentral; PoCG = postcentral; Bankssts = banks of the superior temporal sulcus; CerebC = cerebellum. No CThk increases were observed. The Mann-Whitney U test was applied with significance $p<0.05$.

and Rh-STG and Rh-PCn. These regions have been recently associated with differences in cortical thicknesses observed between these two groups of patients [35].

F. Connectivity Analysis EMCI vs AD

In this test, the observed differences are similar to the ones found in the comparison between CTRL and AD groups. The main differences include the extension of changes of the ERC

and PHG regarding decrease in GMV and CThk and increase in MD, suggesting that these structures are particularly affected in the progression from EMCI to AD. As before, the Lh-MeOFC appears to have a role in disease progression, as it is known to have strong connections to the hippocampus and the ERC and participate in decision-making and reward cognitive processes [36], [37].

Interestingly, a bilateral Deg decrease in the precentral gyrus (PCG) and the Acc was observed. The latter also showed increased rSUV. This suggests that PCG changes may be associated with known gait variability in MCI and AD patients [38] and increased changes in Acc [37].

Finally, decreases in rSUV were also observed for Hip bilaterally and for Rh-Tha, and also several inter-hemispheric connections were observed to be reduced.

G. Connectivity Analysis LMCI vs AD

It can be observed that the main differences between groups are related to a higher predominance of changes in temporal regions such as the Hip and the ITG, and also of the SMG and the Acc. Interestingly, the GMV observed to be decreased bilaterally for the pars orbitalis may be related to known deficits in semantic fluency [39], [40].

Once more, the Hip showed decreased rSUV with bilateral decreasing number of fiber connections, which may translate an increased damage to this structure.

H. Overall Connectivity changes in AD

Although this study is preliminary and based in a small cohort, the obtained results are in agreement with the main known findings regarding AD, such as: a decrease of both GMV and CThk [41], and an increase of the MD in temporal, frontal and parietal regions [42], [43]; an increasingly compromised whole-brain structural connectivity [44], [45]; and also a generalized increase in the accumulation of beta-amyloid plaque [46], [47]. Moreover, our preliminary results showed a low sensitivity of the 18F-AV-45 radiotracer for differentiation between CTRL-EMCI and LMCI-AD; and a reduction of fiber connectivity with the progression of the disease, especially for intra-hemispherical connections.

This study is also in agreement with a very recent study [48] in which a related dataset and connectivity analysis were also used. The authors of this study concluded that the beta-amyloid burden, as measured by 18F-AV-45, was related to changes in structural connectivity metrics.

In addition, it was shown that the MIBCA toolbox is a framework suitable for automated processing and comprehensive analysis of multimodal data, with the potential to facilitate the discovery of new aspects of physiopathology and novel biomarkers of disease.

IV. Conclusion

The potential of the MIBCA toolbox for the automatic pre-processing, analysis, visualization and integration, of neuroimaging data applied to the study of AD was presented. The findings obtained using the toolbox were in agreement with the literature for AD. In addition, significant differences in both imaging and connectivity metrics found in group comparisons, such as in CTRL vs EMCI, warrant further investigations which may lead to the identification of biomarkers for early AD diagnosis.

In resume, the MIBCA toolbox can integrate multimodal information without increasing the workload of the researcher. The researcher is only required to manually place the imaging data in the specified hierarchy, defining the different contrasts and regression variables, and then select, in the toolbox's interface, the data types and the analyses to be performed. The following pre-processing and analyses is done automatically in batch. The researcher is finally able to explore the data through an integrated visualization tool. These features make the toolbox especially useful for novel and improved studies where multimodal information is presented, such as in hybrid MR/PET scanners.

Acknowledgment

Data collection and sharing for this project was funded by the Alzheimer's Disease Neuroimaging Initiative (ADNI) (National Institutes of Health Grant U01 AG02418) and DOD ADNI (Department of Defense award number W81XWH-12-2-0012). ADNI is funded by the National Institute on Aging, the National Institute of Biomedical Imaging and Bioengineering, and through generous contributions from the following: Alzheimer's Association; Alzheimer's Drug Discovery Foundation; BioClinica, Inc.; Biogen Idec Inc.; Bristol-Myers Squibb Company; Eisai Inc.; Elan Pharmaceuticals, Inc.; Eli Lilly and Company; F. Hoffmann-La Roche Ltd and its affiliated company Genentech, Inc.; GE Healthcare; Innogenetics, N.V.; IXICO Ltd.; Janssen Alzheimer Immunotherapy Research & Development, LLC.; Johnson & Johnson Pharmaceutical Research & Development LLC.; Medpace, Inc.; Merck & Co., Inc.; Meso Scale Diagnostics, LLC.; NeuroRx Research; Novartis Pharmaceuticals Corporation; Pfizer Inc.; Piramal Imaging; Servier; Synarc Inc.; and Takeda Pharmaceutical Company. The Canadian Institutes of Health Research is providing funds to support ADNI clinical sites in Canada. Private sector contributions are facilitated by the Foundation for the National Institutes of Health (www.fnih.org). The grantee organization is the Northern California Institute for Research and Education, and the study is coordinated by the Alzheimer's Disease Cooperative Study at the University of California, San Diego. ADNI data are disseminated by the Laboratory for Neuro Imaging at the University of Southern California.

References

[1] M. Catani *et al.*, "Connectomic approaches before the connectome," *NeuroImage*, vol. 80, pp. 2–13, 2013.

[2] S. Mori *et al.*, "Three-dimensional tracking of axonal projections in the brain by magnetic resonance imaging," *Annals Neurology*, vol. 45, no. 2, pp. 265–9, 1999.

[3] S. Ogawa *et al.*, "Brain magnetic resonance imaging with contrast dependent on blood oxygenation," *PNAS USA*, vol. 87, pp. 9868–72, 1990.

[4] T. E. J. Behrens and O. Sporns, "Human connectomics," *Current Opinion in Neurobiol.*, vol. 22, pp. 144–53, 2012.

[5] P. J. Toussaint *et al.*, "Resting state FDG-PET functional connectivity as an early biomarker of alzheimer's disease using conjoint univaritate and independent component analyses," *Neuroimage*, vol. 63, pp. 936–46, 2012.

[6] K. A. Johnson *et al.*, "Florbetapir (F18-AV-45) PET to assess amyloid burden in Alzheimer's disease dementia, mild cognitive impairment, and normal aging," *Alzheimers Dement*, vol. 9, pp. S72–83, 2013.
[7] Z. Cui *et al.*, " Panda: A pipeline toolbox for analyzing brain diffusion images," *Front. Hum. Neurosci.*, vol. 7, no. 42, pp. 1–16, 2013.
[8] J. A. Brown *et al.*, "The UCLA multimodal connectivity database: A web-based platform for brain connectivity matrix sharing and analysis," *Front. Neuroinformatics*, pp. 6–28, 2012.
[9] P. Marques *et al.*, "Braincat–a tool for automated and combined functional magnetic resonance imaging and diffusion tensor imaging brain connectivity analysis," *Front. Hum. Neurosci.*, vol. 7, pp. 1–11, 2013.
[10] A. Santos Ribeiro *et al.*, "Multimodal imaging brain connectivity analysis," *MAGMA*, vol. 26, no. S1, p. 232, 2013.
[11] L. Lacerda *et al.*, "Multimodal imaging brain connectivity analysis toolbox," in *Proc. Int. Soc. Magn. Reson. Med*, 2014, vol. 22, p. 3003.
[12] B. Fischl, "Free surfer," *NeuroImage*, vol. 62, pp. 774–81, 2012.
[13] S. M. Smith *et al.*, "Advances in functional and structural MR image analysis and implementation as FSL," *Neuroimage*, vol. 23, pp. S208–19, 2004.
[14] J. Ashburner and K. J. Friston, "SPM," *Hum. Brain Mapp.*, vol. 7, pp. 254–66, 1999.
[15] R. Wang *et al.*, "Diffusion Toolkit: A software package for diffusion imaging data processing and tractography," in *Proc. Int. Soc. Magn. Reson. Med.*, 2007, vol. 15, p. 3720.
[16] M. Rubinov and O. Sporns, "Complex network measures of brain connectivity: Uses and interpretations," *NeuroImage*, vol. 52, pp. 1059–69, 2010.
[17] A. Santos Ribeiro *et al.*, "Multimodal imaging brain connectivity analysis toolbox (MIBCA)," *PeerJ PrePrints*, vol. 2, p. e699v1, 2014.
[18] A. Bakkour *et al.*, "The effects of aging and alzheimer's disease on cerebral cortical anatomy: Specificity and differential relationships with cognition," *Neuroimage*, vol. 76, pp. 332–44, 2013.
[19] J. Dukart *et al.*, "Relationship between imaging biomarkers, age, progression and symptom severity in Alzheimer's disease," *NeuroImage: Clinical*, vol. 3, pp. 84–94, 2013.
[20] G. Chételat *et al.*, "Direct voxel-based comparison between grey matter hypometabolism and atrophy in Alzheimer's disease," *Brain*, vol. 131, pp. 60–71, 2008.
[21] L. Zhuang *et al.*, "Microstructural white matter changes, not hippocampal atrophy, detect early amnestic mild cognitive impairment," *PloS One*, vol. 8, p. e58887, 2013.
[22] G. W. Van Hoesen *et al.*, "Orbitofrontal cortex pathology in Alzheimer's disease," *Cerebral Cortex*, vol. 10, pp. 243–51, 2000.
[23] M. Pievani *et al.*, "Striatal morphology in early-onset and late-onset Alzheimer's disease: A preliminary study," *Neurobiol. Aging*, vol. 34, pp. 1728–39, 2013.
[24] M. Tondelli *et al.*, "Structural MRI changes detectable up to ten years before clinical Alzheimer's disease," *Neurobiol. Aging*, vol. 33, pp. 825–e25, 2012.
[25] G. Prasad *et al.*, "Brain connectivity and novel network measures for Alzheimer's disease classification," *Neurobiol. Aging*, vol. 36, pp. S121–S131, 2015.
[26] G. Prasad *et al.*, "Tractography density and network measures in Alzheimer's disease," in *2013 IEEE 10th Intern. Symp. Biomed. Imag. (ISBI)*, 2013, pp. 692–695.
[27] J. L. Whitwell *et al.*, "3D maps from multiple MRI illustrate changing atrophy patterns as subjects progress from mild cognitive impairment to Alzheimer's disease," *Brain*, vol. 130, no. 7, pp. 1777–1786, 2007.
[28] J. Shao *et al.*, "Prediction of Alzheimer's disease using individual structural connectivity networks," *Neurobiol. Aging*, vol. 33, pp. 2756–65, 2012.
[29] M. Pievani *et al.*, "Brain connectivity in neurodegenerative diseases—From phenotype to proteinopathy," *Nat. Rev. Neurol.*, vol. 10, pp. 620–33, 2014.
[30] C. C. Rowe *et al.*, "Imaging β-amyloid burden in aging and dementia," *Neurology*, vol. 68, pp. 1718–1725, 2007.
[31] V. Camus *et al.*, "Using PET with 18F-AV-45 (florbetapir) to quantify brain amyloid load in a clinical environment," *Eur. J. Nucl. Med. Mol. Imag.*, vol. 39, pp. 621–631, 2012.
[32] A. Fellgiebel and I. Yakushev, "Diffusion tensor imaging of the hippocampus in MCI and early Alzheimer's disease," *J. Alzheimer's Dis.*, vol. 26, no. S3, pp. 257–62, 2011.
[33] T. Stoub *et al.*, "Parahippocampal white matter volume predicts Alzheimer's disease risk in cognitively normal old adults," *Neurobiol. Aging*, vol. 35, pp. 1855–61, 2014.
[34] H. Cho *et al.*, "Shape changes of the basal ganglia and thalamus in Alzheimer's disease: A three-year longitudinal study," *J. Alzheimer's Dis.*, vol. 40, pp. 285–95, 2014.
[35] B. S. Ye *et al.*, "Comparison of cortical thickness in patients with early-stage versus late-stage amnestic mild cognitive impairment," *Eur. J. Neurol.*, vol. 21, pp. 86–92, 2014.
[36] R. Elliot *et al.*, "Neuroimaging and orbitofrontal cortex," *Cerebral Cortex*, vol. 10, pp. 308–17, 2000.
[37] M. L. Kringelbach, "The human orbitofrontal cortex: Linking reward to hedonic experience," *Nat. Rev. Neurosci.*, vol. 6, pp. 691–702, 2005.
[38] O. Beauchet *et al.*, "Gait variability at fast-pace walking speed: A biomarker of mild cognitive impairment," *J. Nutri. Health Aging*, vol. 17, pp. 235–9, 2013.
[39] J. Eastman *et al.*, "Cortical thickness and semantic fluency in Alzheimer's disease and mild cognitive impairment," *Amer. J. Alzheimer's Dis.*, vol. 1, pp. 81–92, 2013.
[40] M. Catani *et al.*, "A novel frontal pathway underlies verbal fluency in primary progressive aphasia," *Brain*, vol. 136, pp. 2619–28, 2013.
[41] R. Duara *et al.*, "Medial temporal lobe atrophy on MRI scans and the diagnosis of Alzheimer disease," *Neurol.*, vol. 71, pp. 1986–92, 2008.
[42] J. Acosta-Cabronero *et al.*, "Diffusion tensor metrics as biomarkers in Alzheimer's disease," *PloS One*, vol. 7, p. e49072, 2012.
[43] A. Fellgiebel and I. Yakushev, "Diffusion tensor imaging of the hippocampus in MCI and early alzheimer's disease," *J. Alzheimer's Dis.*, vol. 26, pp. 257–262, 2011.
[44] M. Pievani *et al.*, "Assessment of white matter tract damage in mild cognitive impairment and Alzheimer's disease," *Hum. Brain. Mapp.*, vol. 31, pp. 1862–75, 2010.
[45] H. Huang *et al.*, "Distinctive disruption patterns of white matter tracts in alzheimer's disease with full diffusion tensor characterization," *Neurobiol. Aging*, vol. 33, pp. 2029–45, 2012.
[46] H. Engler *et al.*, "Two-year follow-up of amyloid deposition in patients with Alzheimer's disease," *Brain*, vol. 129, pp. 2856–2866, 2006.
[47] A. Forsberg *et al.*, "PET imaging of amyloid deposition in patients with mild cognitive impairment," *Neurobiol. Aging*, vol. 29, pp. 1456–65, 2008.
[48] J. W. Prescott *et al.*, "The Alzheimer structural connectome: Changes in cortical network topology with increased amyloid plaque burden," *Radiol.*, vol. 273, pp. 175–184, 2014.